Nanoscale

Accepted Manuscript

This article can be cited before page numbers have been issued, to do this please use: H. Cha, J. Lee, L. R. Jordan, S. H. Lee, S. Oh, H. J. Kim, J. Park, S. Hong and H. Jeon, *Nanoscale*, 2015, DOI:

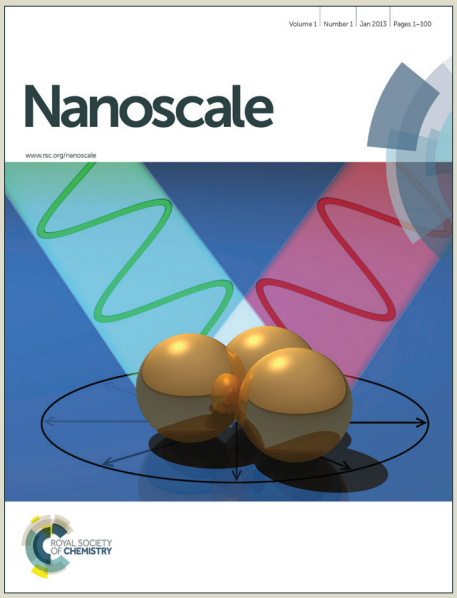

ROYAL SOCIETY OF CHEMISTRY

www.rsc.org/nanoscale

View Article Online
DOI: 10.1039/C4NR07552H

Nanoscale

RSCPublishing

PAPER

Surface passivation of photonic crystal band-edge laser by atomic layer deposition of SiO_2 and its application for biosensing

Cite this: DOI: 10.1039/x0xx00000x

Received ooth January 2012,
Accepted ooth January 2012

DOI: 10.1039/x0xx00000x

www.rsc.org/

Hyungrae Cha,[ab] Jeongkug Lee,[bc†] Luke R. Jordan,[d] Si Hoon Lee,[d‡] Sang-Hyun Oh,[de] Hyo Jin Kim,[f] Juhun Park,[c] Seunghun Hong,[ac] and Heonsu Jeon*[abc]

We report on the conformal surface passivation of photonic crystal (PC) laser devices with an ultrathin dielectric layer. Air-bridge-type Γ-point band-edge lasers (BELs) are fabricated by forming a honeycomb lattice two-dimensional PC structure into an InGaAsP multiple-quantum-well epilayer. Atomic layer deposition (ALD) is employed for conformal deposition of a few-nanometer-thick SiO_2 layer over the entire device surface, not only the top and bottom surfaces of the air-bridge membrane but also the air-hole sidewalls. Despite its extreme thinness, the ALD passivation layer is found to protect the InGaAsP BEL devices from harsh chemicals. In addition, the ALD-SiO_2 is compatible with the silane-based surface chemistry, which allows us to use the ALD-passivated BEL devices as a label-free biosensor. The standard streptavidin–biotin interaction shifts the BEL lasing wavelength by ~1 nm for the dipole-like Γ-point band-edge mode. A sharp lasing line (< 0.2 nm, full width at half-maximum) and large refractive index sensitivity (~163 nm/RIU) produce a figure of merit as high as ~800 for our BEL biosensor, which is at least an order of magnitude higher than those of more common biosensors that rely on a broad resonance peak, showing that our nanolaser structures are suitable for highly sensitive biosensor applications.

1. Introduction

Biosensors using mechanical,[1–3] electrical,[4–6] and optical,[7, 8] transduction mechanisms have been developed for various applications. Among these, optical (or photonic) biosensors have unique advantages over other types of sensor; they are nondestructive and robust against irrelevant changes in the properties of the assay solution, such as its electrical conductivity, salt concentration, or pH values. Optical biosensors are also compatible with optofluidics technology, so a complete sensing system with in situ detection and analysis capabilities can be built in a compact and versatile format. It has been proven that optical resonances in micro- and nanostructures, such as a microdisk,[9] a microring,[10] a grating,[11] a photonic crystal (PC),[12–14] and nanoplasmonics,[15–17] can dramatically improve the sensitivity via strong light–matter interactions.

Rapid progress has been made in the structural designs and performance characteristics of PC-based nanolasers, making them quite promising as compact coherent light sources of the future.[18, 19] For PC-based nanolasers to become a viable device platform, however, a number of issues need to be resolved, which include electrical injection,[20] continuous-wave operation,[21] and high-power operation.[22] For biological applications, the extremely sharp resonance peak makes PC-based nanolasers an ideal platform for building highly sensitive biosensors. However, some reactive chemicals may damage the PC structures, which has been a stumbling block limiting practical applications of PC-nanolaser-based biosensors. In this study, we employed atomic layer deposition (ALD) to deposit an ultrathin (on the scale of a few nanometers) and conformal SiO_2 layer that completely encapsulates a suspended air-bridge-type two-dimensional (2D) PC nanolaser structure having a complex topography. The resultant nanolasers were found to be resistant to wet chemicals that would otherwise instantly damage the compound-semiconductor-based delicate nanolaser structure. As a proof of concept to show the effectiveness and significance of ALD passivation, we demonstrate a highly sensitive label-free biosensor using the ALD-passivated PC nanolasers. Significantly, the biosensor based on our nanolasers takes advantage of the extremely sharp resonance peak of PC nanolasers and exhibits a figure of merit (FOM) of ~800, which is at least 10 times larger than those of previous optical biosensors based on rather broad resonance peaks. This result clearly shows that our strategy is a viable method of building highly sensitive biosensors based on PC nanolaser structures.

View Article Online
DOI: 10.1039/C4NR07332H
Journal Name

2. Photonic crystal band-edge laser

Among the various PC-based nanolaser structures available, we chose a band-edge laser (BEL) in this study; it was constructed in the form of an air-bridge membrane slab composed of an InGaAsP multiple quantum well (MQW) epilayer with a 2D honeycomb lattice array of air holes. A BEL, especially when operated at the Γ point, has several advantages over a defect-containing cavity-based PC laser structure; it has a large modal volume (and thus a high output power) and yields vertical laser emission, both properties facilitating the detection of laser emission off of the wafer plane. In addition, a BEL has an infinite translational symmetry, so the delicate optical alignment procedure required for exciting a cavity-based PC laser can be greatly simplified or omitted.

As for the PC pattern, we fixed the air-hole radius at $r = 0.35a$, where a is the lattice constant of the honeycomb lattice PC. Fig. 1(a) shows the photonic band structure of the honeycomb lattice 2D PC, which was calculated using the plane wave expansion method. There are two closely spaced band-edge modes at the Γ point in the frequency range of $0.25 < a/\lambda < 0.30$. From computer simulations of optical mode profiles, we have found that the two band edges correspond to a dipole-like mode at Γ_2 ($a/\lambda \approx 0.29$) and a monopole-like mode at Γ_1 ($a/\lambda \approx 0.26$). The corresponding mode profiles are shown in Figs. 1(b) and 1(c), respectively. By simply adjusting the lattice constant of the PCs, we could make the optical gain band of the InGaAsP MQWs match either of the two band-edge modes: $a \approx 450$ nm for the dipole-like Γ_2 mode and $a \approx 400$ nm for the monopole-like Γ_1 mode.

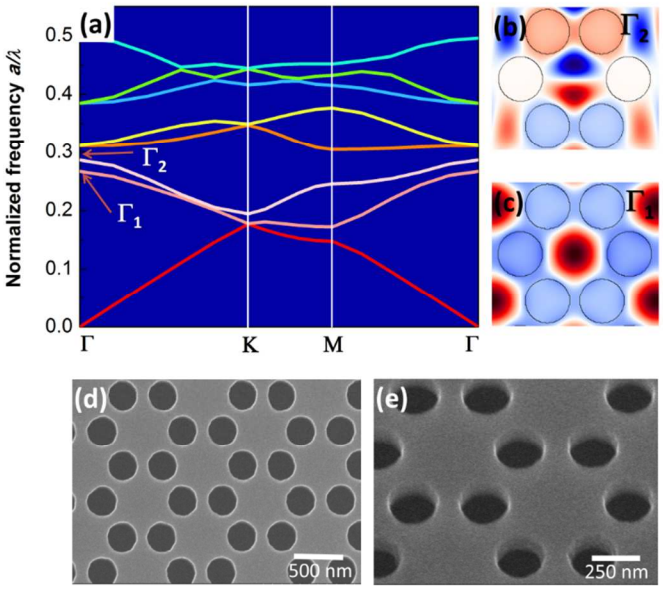

Fig. 1. (a) Photonic band structure of a 2D honeycomb lattice PC. Magnetic field (H_z) distribution patterns calculated at the two Γ points: (b) dipole-like Γ_2 mode and (c) monopole-like Γ_1 mode. SEM images of a 2D honeycomb lattice PC fabricated in an air-bridge format: (d) top view and (e) tilted view at a higher magnification.

The base wafer from which the PC BEL structure was constructed was a standard InGaAsP MQW structure with the emission wavelength $\lambda \sim 1550$ nm. Inserted underneath the MQW layer were a 1-μm-thick InP etch-sacrificial layer and an InGaAs etch-stop layer. The InP sacrificial layer has a high wet-etch selectivity over both the InGaAsP MQW layer on top and the underlying InGaAs etch-stop layer, enabling the formation of an MQW air-bridge slab that serves as a waveguide along the wafer plane. A thin Si_3N_4 layer was deposited onto the base wafer and used as a hard mask layer during PC pattern generation into the MQW slab by a combination of electron beam lithography and reactive ion etching (RIE). After the Si_3N_4 hard mask layer was removed by dry etching, the InP etch-sacrificial layer was selectively wet-etched through the PC air holes to finish the BEL structure in the air-bridge format. Figs. 1(d) and 1(e) show scanning electron microscope (SEM) images of a completed PC BEL structure.

3. ALD surface passivation

Our air-bridge BEL structure with a 2D array of air holes has a high surface-to-volume ratio (SVR) and is thus intrinsically suitable for sensing applications where a strong overlap between the internal optical resonance mode and the external environmental medium is highly desirable. A high SVR, however, implies a substantial semiconductor surface area to be exposed, which requires appropriate surface protection to keep the BEL device from disruptive environmental substances that may be encountered. The problem is compounded because InP-based semiconductor materials are known to be readily dissolved in many chemicals.[23] In addition, exposed bare semiconductor surfaces result in a large number of dangling bonds and subsequent extrinsic defects, which usually act as nonradiative surface recombination centers that cause rapid carrier annihilation.[24] Therefore, a certain form of surface passivation should be beneficial for both short-term and long-term performance of BEL devices.

Various surface passivation methods have been developed for optoelectronic devices based on compound semiconductors, such as chemical treatment,[25] thermal treatment,[26] and physical deposition of a thin dielectric film.[27] Among these, thin film deposition provides a physically secure and stable means of device protection. However, the deposited layer has to be very thin–preferably down to an atomic layer–in order to fully exploit the strong overlap between an optical mode and an outer medium crucial for high sensitivity in sensing. Here we employed an ALD technique to coat the entire exposed surface of an air-bridge InGaAsP MQW PC BEL device with a uniform and conformal layer of SiO_2 film only a few nanometers thick. ALD is a thin film deposition technique that uses self-saturating chemical adsorption and substitution of molecules to deposit an atomically thin film layer. Because gas-phase precursors in ALD reactions can reach places that would be inaccessible with any physical deposition technique, ALD is particularly useful for depositing a thin film uniformly and conformally on

View Article Online
DOI: 10.1039/C4NR07532H

substrates with challenging topography, such as deep high-aspect-ratio trenches, sidewalls, or suspended films. When applied to our PC laser structure, the ALD process allows gas molecules to reach even the underside of the air-bridge membrane through the open air holes that constitute the PC pattern, resulting in the deposition of a uniform passivation layer not only on the top surface but also on the sidewalls as well as the bottom face of the MQW slab, yet with a nanometer-scale precision in the film thickness.

First, we deposited a few-nanometer-thick SiO_2 film on an InP bare wafer by following the ALD procedure described in reference 28, Im *et al*. We controlled the deposition cycles to obtain a desired film thickness of ~1 nm, having obtained the deposition rate per cycle from ellipsometer measurements of a calibration sample on which multiple cycles of the ALD process were performed. Fig. 2(a) shows a transmission electron microscope (TEM) image taken for a nominally 5-nm-thick ALD-SiO_2 film, which presents direct visual evidence that a dielectric film of nanometer-scale was indeed deposited. To test its durability and ability to protect the underlying InP, we then defined an array of circular photoresist patterns 400 μm in diameter using conventional photolithography. A sample prepared in this way was immersed in a buffered oxide etchant for 20 s to remove the ALD-SiO_2 film from the regions uncovered with photoresist, which was followed by photoresist stripping in acetone. The sample was then soaked for 30 s in a dilute HCl solution ($HCl:H_2O$ = 3:1), which is known to be a very efficient InP etchant. Fig. 2(b) shows an SEM image of a circular mesa that was formed after HCl immersion. The InP substrate was etched to a depth of ~3 μm in the region where the ALD-SiO_2 layer was absent, whereas the circular region defined and passivated by the ALD-SiO_2 layer remained perfectly intact. This is solid evidence that the ALD-SiO_2 film protects the underlying InP from extremely harsh environments, despite its diminishingly negligible thickness.

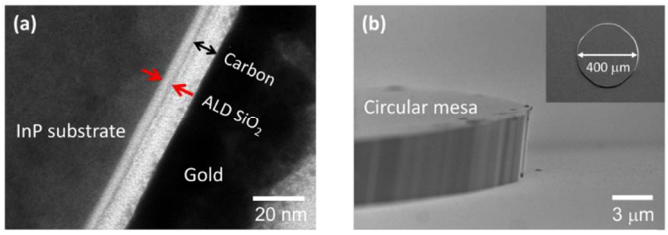

Fig. 2. (a) Cross-sectional TEM image of an ALD-SiO_2 layer deposited on an InP bare substrate. Carbon and gold layers were added on top of the ALD-SiO_2 layer during TEM specimen preparation. (b) SEM image of an InP circular mesa etched in a diluted HCl solution with the mesa top protected by the ALD-SiO_2 layer. Inset is another SEM image of the circular mesa taken from the top.

Encouraged by the initial test on the bare InP substrate, we applied the ALD-SiO_2 passivation to our BEL devices. A nominally 5-nm-thick SiO_2 film was deposited onto the aforementioned air-bridge Γ-point BEL structure. We then immersed the sample in piranha solution ($H_2SO_4:H_2O_2:H_2O$ = 1:1:10) for two full minutes, which guarantees complete etching of the thin InGaAsP MQW layer (and thereby destruction of the entire membrane structure) unless the ALD-SiO_2 layer efficiently protects the InGaAsP material from the etchant. Visual inspection under an optical microscope revealed that the PC BEL devices remained intact even after the intentional etch trial, without any visual change in the air-bridge membrane structure. After the visual test, we operated the PC BELs to examine their lasing performance characteristics. Each individual BEL device was pumped using a 980 nm pulsed laser diode (20 ns pulse width and 1% duty cycle), and optical emission from the device was fed into an optical spectrum analyzer. Fig. 3(a) shows lasing spectra of a typical Γ_2 BEL device recorded at different sample treatment stages: as fabricated, after ALD-SiO2 layer deposition, and after 2 min treatment in piranha solution.

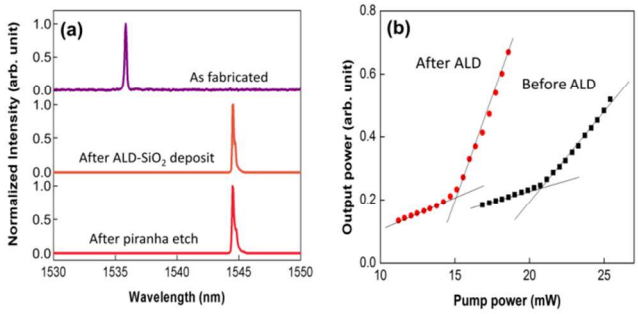

Fig. 3. (a) Lasing spectra from an InGaAsP MQW Γ_2 BEL device, taken at different stages of sample treatment: (from top) as-fabricated, after 5-nm-thick ALD-SiO_2 layer deposition, and after subsequent 2 min wet etch in piranha solution. For clarity, the spectra are shifted in the vertical direction. (b) Output power versus input power relations of a typical Γ_2 BEL device measured before and after 5 nm ALD-SiO_2 layer deposition

Although the ALD-SiO_2 layer deposition caused a sizable redshift ($\Delta\lambda$ ~ 8.7 nm) in the lasing peak position, which was due to the increase in the effective refractive index of the device, the subsequent 2 min piranha solution treatment had absolutely no effect on the lasing peak position. This result is strong evidence that the 5-nm-thick ALD-SiO_2 layer provides an ideal means of device protection from harsh chemicals. In fact, we noticed that the BEL devices performed even better after the ALD-SiO_2 layer deposition, as shown in Fig. 3(b): their lasing threshold decreased by ~30%, and the slope efficiency more than doubled. We believe that these results are due to partial remedying of dangling bonds by the ALD process, which in turn reduces the number of nonradiative recombination centers. The detailed mechanisms of the improved laser performance will be the subject of further investigation in the future.

4. Biochemical sensing results and discussion

We examined the possibility of using the ALD-SiO_2-passivated PC BEL devices for biosensing applications. Many biosensing methods rely on the interactions between ligands and receptors. Label-free biosensing applications require a highly sensitive transducer device that responds directly to the ligand–receptor interaction and generates large sensing signals. Therefore,

View Article Online
DOI: 10.1039/C4NR07332H Journal Name

transducer devices based on nanophotonic principles are attractive candidates because they offer a large signal change due to not only their large SVR but also their strong field enhancement effect at spatially localized spots or regions. Biosensing devices often undergo treatments or preparation steps that involve rather harsh chemicals, some of which may be harsh enough to damage these small devices. An appropriate solution to this potential problem can be conformal deposition of a surface passivation layer, preferably a very thin layer if the local field enhancement effect of nanophotonic devices is to be fully exploited. The ALD process fulfills these conditions; it can coat all the exposed surfaces regardless of the shape and configuration of the device, and yet it can control the thickness down to a few nanometers. It should be mentioned that in this study we employed an ALD-SiO_2 layer, not an ALD-Al_2O_3 layer that is far more common in the ALD community. In fact, we intentionally chose ALD-SiO_2 because the common silane-based chemistry, which has been developed specifically for a SiO_2-terminated surface such as glass or SiO_2-deposited wafers, can then be readily used.

As a proof-of-concept experiment, we performed biosensing experiments in which our PC nanolaser was first surface-functionalized with biotin molecules and then exposed to streptavidin molecules so that the streptavidin–biotin interaction could occur. The streptavidin–biotin interaction is well known to form a strong noncovalent bond (dissociation constant $K_d \approx 10^{-15}$ M) and to provide consistent binding results without being affected by the experimental conditions, such as the pH, temperature, and presence of organic solvents or other agents. Because of these bonding characteristics, the complex has been used in many biological applications such as protein and nucleic acid detection and purification methods.[29, 30] The overall sample preparation procedure is schematically outlined in Fig. 4(a); the details are deferred to the Experimental Section. The ratio of biotin-PEG to PEG was controlled so that only ~10% of the surface was functionalized. Although our device should work as a label-free sensor, we intentionally attached fluorescing dye molecules to streptavidin so that we could evaluate the quality of the biotinylation on the ALD-SiO_2 surface using fluorescence microscopy. Fig. 4(b) shows a fluorescence image captured after the streptavidin–biotin interaction was complete. The PC-patterned regions, which are filled with air holes and thus have a high SVR, obviously exhibited much stronger fluorescence intensity than the planar region with no PC pattern, confirming that the overall surface chemistry was properly realized.

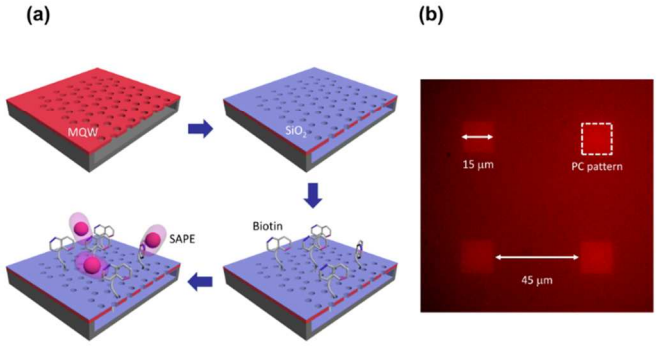

Fig. 4. (a) Schematic surface functionalization steps for biosensing test. From top-left: 2D PC BEL fabrication; conformal deposition of ALD-SiO_2 layer; biotinylation of silica-terminated surface; and chemical interaction between biotin and streptavidin molecules tagged with phosphor (SAPE). (b) Fluorescence microscopy image taken after the dye-conjugated streptavidin was bound onto the biotin-functionalized PC surface.

Lasing spectra of the ALD-SiO_2-passivated PC BELs were measured at various stages of the streptavidin–biotin interaction process. Fig. 5 shows typical lasing spectra before and after the streptavidin–biotin binding for both the dipole-like and monopole-like BEL modes. The BEL peaks shifted by ~0.95 nm for the dipole-like mode and by ~0.80 nm for the monopole-like mode; similar spectral redshifts were consistently measured for all the BEL devices in the same batch. The measured results indicate that our PC BELs are quite competitive when compared with other nanophotonics-based sensors. For instance, plasmonic resonance occurring in a Ag nanohole array was reportedly redshifted by ~1.3 nm for a 10% biotinylated surface[31]; although the sensing mechanisms are totally different, the magnitudes of the resonance shifts are of the same order, implying similar sensitivities. The spectral peak shift for the dipole-like mode was slightly larger than that for the monopole-like mode; we attribute this to the fact that the dipole-like mode is somewhat larger, and consequently its electric field extends further into the air holes, which makes the dipole-like mode respond to the environmental change more strongly, leading to a higher sensitivity.[32]

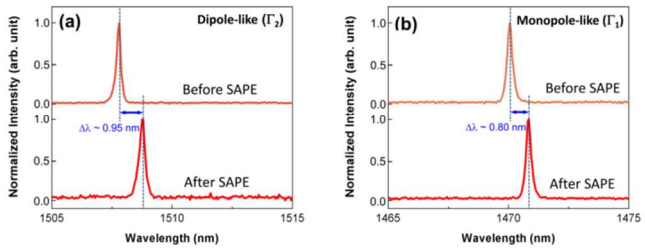

Fig. 5 Streptavidin sensing experiments in which lasing spectra of biotin-functionalized BEL biosensors were measured before and after streptavidin molecules were applied to the biosensors. Graphs show the lasing spectra of the biosensors in (a) dipole-like Γ2 BEL mode and (b) monopole-like Γ1 BEL mode. Spectra in each plot are vertically shifted for clarity.

In addition to the positive control samples described above, we also prepared and counter-checked negative control

View Article Online
DOI: 10.1039/C4NR07532H

samples, for which the biotin-PEG process was replaced with bare PEG (without biotin) so that streptavidin–biotin binding could not occur, leaving the nanolaser surface without any streptavidin molecules. In good contrast, the negative control samples exhibited no measurable spectral shift for either type of band-edge mode within the resolution limit (0.05 nm) of the optical spectrum analyzer we used for the measurements, as shown in Fig. 6. By taking the ratio of the peak shifts between the positive and negative control samples, we obtained a signal-to-noise ratio of greater than 20 for streptavidin sensing using our biotin-functionalized PC nanolasers in a dipole-like mode, which is large enough to ascertain that streptavidin–biotin binding occurred.

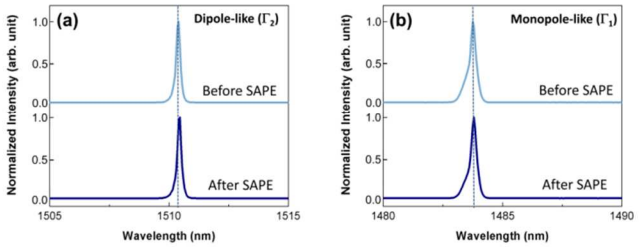

Fig. 6. Negative control experiments in which the lasing spectra of BEL devices *without biotin* were measured *before* and *after* streptavidin molecules were applied to the devices. Graphs show the lasing spectra of the (biotin-free) BEL devices in (a) dipole-like Γ_2 BEL mode and (b) monopole-like Γ_1 BEL mode. Spectra in each plot are vertically shifted for clarity.

One common parameter used to quantify the quality of an optical biosensor is the FOM, which is defined as the refractive index sensitivity (i.e., the wavelength shift per unit refractive index change) divided by the linewidth of the resonance peak at full width at half-maximum (FWHM). We performed band structure calculations for our honeycomb lattice 2D PC BEL structure to evaluate the rate at which the band edge shifts as the refractive index of the environmental medium is increased, from which we estimated the index sensitivity of our device to be ~163 nm/RIU (RIU: refractive index unit) for the dipole-like mode. Because the measured FWHM linewidth of our BEL lasing peak was ~0.2 nm, the FOM of our dipole-like BEL mode is as high as ~800. This FOM value is much larger than those of previous sensors that rely on a rather broad resonance peak, such as surface plasmon resonance (SPR).[8, 33]

5. Experimental

Device Fabrication: The InGaAsP MQW structure was grown on an n-type (001)-oriented InP substrate by a low-pressure metal-organic chemical vapor deposition system. Grown sequentially on the n-InP substrate were an InP buffer layer, a 50-nm-thick InGaAs etch-stop layer, a 1000-nm-thick InP sacrificial layer, and finally a 230-nm-thick MQW layer composed of five pairs of an 8-nm-thick InGaAsP quantum well and a 20-nm-thick InGaAsP barrier. A 50-nm-thick Si_3N_4 hard mask layer was deposited on the InGaAsP MQW base wafer by plasma-enhanced chemical vapor deposition at 300°C, followed by conventional electron beam lithography to define a 2D honeycomb lattice hole array pattern. The acceleration voltage and electron current during pattern generation were 100 keV and 300 μC/cm2, respectively. RIE was then performed to transfer the PC pattern into the underlying hard mask layer and subsequently into the InGaAsP MQW layer, with gas mixtures of CF_4/O_2 for Si_3N_4 and CH_4/H_2 for InGaAsP. After the remaining Si_3N_4 hard mask layer was removed, the sample was finally immersed in diluted HCl ($HCl:H_2O = 3:1$) to selectively remove the InP sacrificial layer underneath the MQW layer, which completed the air-bridge PC nanolaser fabrication.

SiO_2-ALD: Silicon oxide films were deposited by the ALD process on a bare InP substrate and also on the honeycomb lattice 2D PC BEL structure. The overall SiO_2 ALD process was adapted from reference 34, Hausmann *et al*. Two precursors, trimethylaluminum (TMA) and tris(tert-butoxy)silanol, were sequentially pulsed through the reaction chamber; a small amount of Al plays a critical role as a seeding agent for the successful deposition of a Si-dominant oxide layer. First, TMA was pulsed into the chamber for 0.15 s, followed by a N_2 carrier gas with a flow rate of 20 sccm for 5 s to remove the TMA from the chamber. Second, silanol was pulsed into the chamber for 0.5 s and allowed to react for 30 s, followed by the N_2 carrier gas with a flow rate of 20 sccm for 30 s to remove the silanol from the chamber. This sequence, which constituted one ALD cycle of SiO_2 deposition and resulted in an approximately 1-nm-thick SiO_2 layer, was repeated until a desired thickness was deposited. The operating temperature was kept at 250°C throughout the ALD process.

Surface Functionalization: A series of chemical treatments were performed to biofunctionalize the surfaces of the PC BEL device with biotin and subsequently to sense streptavidin on the basis of the streptavidin–biotin interaction. Before the surface chemistry treatments, the device sample went through a standard solvent cleaning procedure and was subsequently treated in piranha solution, which should remove any organic residue on the SiO_2-encapsulated device surface. The sample was then soaked overnight in a 2% solution of (3-aminopropyl) triethoxysilane (APTES) in phosphate buffered saline (PBS) solution, which covered the ALD-SiO_2 terminated sample surface with a self-assembled monolayer of APTES molecules via the self-assembly process. APTES molecules, which are commonly used as a coupling agent, make the SiO_2 surface more favorable to biotin molecules and are widely used in various biological studies, such as those involving protein adhesion and cell growths. After the APTES treatment, the sample was incubated for up to 4 h in a mixture solution of N-hydroxysuccinimide esters of polyethylene glycol (PEG) and biotin-PEG in a 100 mM sodium bicarbonate buffer (pH 8.25) to prepare a partially biotin-terminated surface. Note that the rest of the surface is simply PEG-terminated, which prevents nonspecific binding of streptavidin and ensures that streptavidin binds selectively to the biotin-terminated surface only. We controlled the relative concentrations of PEG and biotin-PEG such that biotin covers ~10% of the total surface area. During the biosensing operation, a drop of 100 nM streptavidin

View Article Online
DOI: 10.1039/C4NR07332H
Journal Name

conjugated with R-phycoerythrin fluorescence dye (SAPE) was applied to the biotin-PEG-terminated sample to induce the streptavidin–biotin interaction. We intentionally used the fluorescently conjugated streptavidin, SAPE, to independently confirm the streptavidin–biotin binding using fluorescence microscopy. Finally, the sample was rinsed in deionized water and dried.

6. Conclusion

In conclusion, we fabricated air-bridge-type 2D PC BELs using an InGaAsP MQW structure and subsequently applied the ALD process to passivate the entire device surface with a few-nanometer-thick conformal SiO_2 layer. Despite its extreme thinness, the ALD-SiO_2 layer was found to protect the devices almost perfectly from harsh chemical environments, whereas noticeable improvement in the lasing performance was an unexpected byproduct. The ALD-SiO_2-passivated BEL devices were tested as a biosensor. By using the streptavidin–biotin reaction, we determined the FOM of the sensor to be ~800, which is at least an order of magnitude higher than that of previous SPR-based sensors. This large FOM is due mainly to the sharp resonance peak resulting from the lasing action. Together with all the advantages of the Γ-point BEL, such as its high output power, vertical laser emission, and relaxed tolerance in optical alignment (due to the infinite translational symmetry of a BEL pattern structure), these preliminary test results pave the way to a compact ultrasensitive biosensor platform based on nanophotonics technology.

Acknowledgements

This work was supported by a National Research Foundation (NRF) grant [2008-0061906] funded by the Ministry of Science, ICT, and Future Planning (MSIP, Korea) and also in part by the Industrial Strategic Technology Development program [10041913] funded by the Ministry of Trade, Industry & Energy (MOTIE, Korea). H.C. is grateful for the financial support by the BK21 PLUS Scholarship sponsored by the Ministry of Education (MOE, Korea). L.R.J. and S.-H.O. acknowledge support from the U.S. National Science Foundation (NSF CAREER Award #DBI 1054191).

Notes and references

[a] Department of Biophysics and Chemical Biology, Seoul National University, Seoul 151-747, Republic of Korea
[b] Interuniversity Semiconductor Research Center, Seoul National University, Seoul 151-747, Republic of Korea
[c] Department of Physics and Astronomy, Seoul National University, Seoul 151-747, Republic of Korea
[d] Department of Biomedical Engineering, University of Minnesota, Minneapolis, MN 55455, USA
[e] Department of Electrical and Computer Engineering, University of Minnesota, Minneapolis, MN 55455, USA
[f] Korea Photonics Technology Institute, Gwangju 500-779, Republic of Korea
[†] Current address: Display Research Center, Samsung Display, Yongin, Gyeonggi 449-711, Korea
[‡] Current address: Creativity & Innovation Center, Samsung Electronics, Yongin, Gyeonggi 446-712, Korea

[*] Corresponding author e-mail: hsjeon@snu.ac.kr

1 N. V. Lavrik, M. J. Sepaniak, and P. G. Datskos, *Rev. Sci. Instrum.*, 2004, **75**, 2229-2253.
2 F. Josse, F. Bender, and R. W. Cernosek, *Anal. Chem.*, 2001, **73**, 5937-5944.
3 A. Janshoff, H.-J. Galla, and C. Steinem, *Angew. Chem. Int. Ed.*, 2000, **39**, 4004-4032.
4 E. Braun, and K. Keren, *Adv. Phys.*, 2004, **53**, 441-496.
5 Y. Cui, Q. Wei, H. Park, and C. M. Lieber, *Science*, 2001, **293**, 1289-1292.
6 H. Im, X. J. Huang, B. Gu, and Y. K. Choi, *Nat. Nanotechnol.*, 2007, **2**, 430-434.
7 M. A Cooper, *Nat. Rev. Drug Discovery*, 2002, **1**, 515-528.
8 J. Homola, *Chem. Rev.*, 2008, **108**, 462-493.
9 T. J. Kippenberg, S. M. Spilane, D. K. Armani, and K. J. Vahala, *Appl. Phys. Lett.*, 2003, **83**, 797-799.
10 I. M. White, H. Zhu, J. D. Suter, N. M. Hanumegowda, H. Oveys, M. Zourob, and X. Fan, *IEEE Sens. J.*, 2007, **7**, 28-35.
11 W. Liang, Y. Huang, Y. Xu, R. K. Lee, and A. Yariv, *Appl. Phys. Lett.*, 2005, **86**, 151122.
12 M. L. Adams, M. Loncar, A. Scherer, and Y. Qiu, *IEEE J. Sel. Areas Commun.*, 2005, **23**, 1348-1354.
13 S. Kita, K. Nozaki, and T. Baba, *Opt. Express*, 2008, **16**, 8174-8180.
14 S. Kita, S. Otsuka, S. Hachuda, T. Endo, Y. Imai, Y. Nishijima, H. Misawa, and T. Baba, *Trans. Inst. Electron. Inf. Commun. Eng. Sect. E.*, 2012, **95**, 188-198.
15 N. C. Lindquist, P. Nagpal, K. M. McPeak, D. J. Norris, and S.-H. Oh, *Rep. Prog. Phys.*, 2012, **75**, 036501.
16 A. G. Brolo, *Nat. Photonics*, 2012, **6**, 709-713.
17 A. Dahlin, N. J. Wittenberg, F. Hook, and S.-H. Oh, *Nanophotonics*, 2013, **2**, 83-101.
18 D. J. Norris, *Nat. Mater.*, 2007, **6**, 177-178.
19 T. Baba, *Nat. Photonics*, 2008, **2**, 465-473.
20 H. G. Park, S. H. Kim, S. H. Kwon, Y. G. Ju, J. K. Yang, J. H. Baek, S. B. Kim, and Y. H. Lee, *Science*, 2004, **305**, 1444-1447.
21 S. Kim, J. Lee, and H. Jeon, *Opt. Express*, 2011, **19**, 1-6.
22 S. Kim, Y. Park, K. Hwang, J. Lee, H. Jeon, and H. J. Kim, *J. Opt. Soc. Am. B*, 2009, **26**, 1330-1333.
23 P. H. Holloway, D. E. McGuire, *Handbook of Compound Semiconductors*, William Andrew Inc., Norwich, NY, 1996.
24 P. T. Landsberg, *Recombination in Semiconductors*, Cambridge University Press, Cambridge, 1991.
25 C. J. Sandroff, R. N. Nottenburg, J.-C. Bischoff, and R. Bhat, *Appl. Phys. Lett.*, 1987, **51**, 33.
26 F. Gao, S. J. Lee, D. Z. Chi, S. Balakumar, and D.-L. Kwong, *Appl. Phys. Lett.*, 2007, **90**, 252904.
27 M. L. Huang, Y. C. Chang, C. H. Chang, Y. J. Lee, P. Chang, J. Kwo, T. B. Wu, and M. Hong, *Appl. Phys. Lett.*, 2005, **87**, 252104.
28 H. Im, N. J. Wittenberg, A. Lesuffleur, N. C. Lindquist, and S.-H. Oh, *Chem. Sci.*, 2010, **1**, 688-696.

Journal Name

View Article Online
DOI: 10.1039/C4NR07532H ARTICLE

29 M. D. Savage, *in A Laboratory Guide to Biotin-labeling in Biomolecule Analysis*, ed. T. Meier and F. Fahrenholz, Birkhäuser Verlag, Basel, 1996, pp. 1–29.

30 N. M. Green, *Biochem J.*, 1963, **9**, 599-609.

31 H. Im, S. H. Lee, N. J. Wittenberg, T. W. Johnson, N. C. Lindquist, P. Nagpal, D. J. Norris, and S.-H. Oh, *ACS Nano*, 2011, **8**, 6244-6253.

32 S. Kim, J. Lee, H. Jeon, and H. J. Kim, *Appl. Phys. Lett.*, 2009, **94**, 133503.

33 Y. Shen, J. Zhou, T. Liu, Y. Tao, R. Jiang, M. Liu, G. Xiao, J. Zhu, Z. K. Zhou, X. Wang, C. Jin, and J. Wang, *Nat. Commun.*, 2013, **4**, 1-9.

34 D. Hausmann, J. Becker, S. Wang, and R. G. Gordon, *Science*, 2009, **298**, 402-406.